Journal of Power Sources 296 (2015) 92–101

Contents lists available at ScienceDirect

Journal of Power Sources

journal homepage: www.elsevier.com/locate/jpowsour

Thermodynamics of sulfur poisoning in solid oxide fuel cells revisited: The effect of H_2S concentration, temperature, current density and fuel utilization

Aline Lima da Silva*, Nestor Cezar Heck

Computational Thermodynamics for Metallurgy and Materials (NTCm Research Group) – Program of Postgraduate Studies in Mining, Metals and Materials Engineering (PPGE3M), Federal University of Rio Grande do Sul – UFRGS, Campus do Vale, Setor 5, Centro de Tecnologia, Sala 222, Av. Bento Gonçalves 9500, CEP 91501-970, Porto Alegre, RS, Brazil

HIGHLIGHTS

- Ni–S Gibbs energy diagram systematizes understanding of sulfur interaction with Ni.
- Whenever sulfur chemical potential is increased, deactivation by sulfur is greater.
- Increasing current density increases the degree of sulfur poisoning of Ni catalyst.
- Current density effect becomes remarkable at fuel utilizations >90%.
- Thermodynamic results are in agreement with recent experimental evidences.

ARTICLE INFO

Article history:
Received 4 April 2015
Received in revised form
9 July 2015
Accepted 15 July 2015
Available online xxx

Keywords:
Thermodynamics
Methane
Internal reforming
Sulfur tolerance
Solid oxide fuel cells

ABSTRACT

Thermodynamics of sulfur poisoning in SOFCs is revisited in the present study, aiming at contributing to the understanding of the effects of different operating parameters on deactivation by sulfur. Ni–S Gibbs energy diagram shows that, whenever sulfur chemical potential is increased, the catalyst poisoning becomes greater, due to increase in nickel sulfide activity, which is a strictly increasing function of sulfur coverage on Ni surface. For studying current density effect, simulations are carried out in the range of 0 (OCV) – 1 A cm^{-2}, at 1123 K, considering methane as a fuel. At 10 ppm H_2S, an increase in current density from 0 (OCV) to 0.5 A cm^{-2} results in a slight increase in the nickel sulfide activity from 3.0×10^{-6} to 1.2×10^{-5}; however, at 1 A cm^{-2}, nickel sulfide activity is 25.000 times higher than at 0.5 A cm^{-2}. At 1 A cm^{-2}, H_2 and CO are almost entirely converted to H_2O and CO_2 by electrochemical reaction. Therefore, the effect of current density becomes remarkable when fuel utilization approaches 100%. These theoretical findings are corroborated by the recent experimental evidences related to the detrimental influence of current density on SOFC performance during sulfur poisoning.

1. Introduction

A great challenge for the commercialization of Solid Oxide Fuel Cells (SOFCs) is the low tolerance of Ni-based anodes to poisonous gases, such as hydrogen sulfide (H_2S), present in hydrocarbon fuels (*e.g.* biogas, natural gas) [1–3]. In this context, sulfur poisoning of SOFCs has been extensively studied for different fuels, such as hydrogen [4–10], methane [2,11,12] and biogas [13,14]. As mentioned by Cheng et al. [3], the factors that critically influence the impact of sulfur on SOFC anodes are H_2S concentration in the fuel, temperature, fuel composition, current density and anode material. Regarding the effect of H_2S concentration and temperature on the degree of sulfur poisoning of SOFC anodes, one can see a general consensus in literature: an increase in H_2S concentration results in a greater anode degradation [4,8], and a decrease in operating temperature leads to a greater deactivation of catalyst [4,5,7,9]. On the other hand, the effect of current density on the impact of sulfur on SOFC anodes is controversially discussed in literature: while several experimental and theoretical studies [6,15–17] suggest that the increase in current density helps to alleviate the sulfur poisoning effect on the anode because of the

* Corresponding author.
E-mail address: adasilva26@gmail.com (A.L. da Silva).

http://dx.doi.org/10.1016/j.jpowsour.2015.07.046
0378-7753/

Nomenclature

G	total Gibbs energy of the system
G_i^0	Gibbs energy of species i at its standard state
μ_i^0	chemical potential of species i at its standard state
$\Delta\mu$	change in chemical potential
$\Delta\overline{\mu}$	change in chemical potential determined from Ni–S Gibbs energy diagram
n_i	number of moles of species i
n_i°	inlet molar flow rate of species i
x_i	molar fraction of species i
a_i	activity of species i
R	gas constant (8.31434 J K^{-1} mol^{-1})
T	temperature of the system
P	total pressure of the system
p_i	partial pressure of species i
M, N	total number of components and species, respectively
δ_{ik}	number of atoms of kth component present in each molecule of species i
b_k	total number of atomic masses of kth component in the system
λ_k	Lagrange's multipliers
θ	sulfur coverage on Ni surface
α	fitting parameter used in Temkin-like isotherms
ΔH	change in enthalpy
ΔS	change in entropy
Rx	reaction (x)
D	driving force for the formation of a condensed phase
K	equilibrium constant
U_f	fuel utilization
j	current density
F	Faraday constant (96,485.34C mol^{-1})
W	power output

higher supply of O^{2-} ions, which contributes to desorption of chemisorbed sulfur from the triple-phase boundary (TPB), a recent experimental investigation carried out by Hagen et al. [18] shows exactly the opposite trend; that is, under internal reforming conditions, the operation at higher current loads results in a greater degradation of SOFC performance during sulfur poisoning. In fact, some previous studies also show that the increase in current density leads to an increase in the detrimental impact of sulfur on the anode. Xia and Birss [10], for example, verified that, for an SOFC operating on wet hydrogen containing 10 ppm H_2S at 1073 K, the degree of sulfur poisoning of anode was greater under current load than during OCV (open-circuit voltage) operation.

Therefore, a consistent theoretical analysis could be helpful for improving the understanding of the effect of different operating parameters (H_2S concentration, temperature, current density, fuel utilization) on the degree of sulfur interaction with Ni. A new thermodynamic study could be particularly useful for clarifying the controversial effect of current density on SOFC anodes during sulfur poisoning. In this way, the present study evaluates, by means of the construction of Ni–S Gibbs energy diagrams, the influence of different operating variables on the interaction of H_2S with Ni catalyst. In our previous work [19], it was demonstrated by using Ni–S–H Gibbs energy diagrams that the incorporation of oxides into Ni-based anodes decreases the sulfur chemical potential and hence lowers the degree of sulfur poisoning of Ni catalyst. From the S–H face of the Gibbs energy diagram, one can see that, due to the shape of the curve of Gibbs energy of the gas phase, even very small variations in the H_2S content are able to produce tangent lines with very different slopes, which significantly alters the values of sulfur chemical potential. In the present research, the analysis is focused on the construction of Ni–S Gibbs energy diagrams, which are explored in greater detail. This kind of diagram allows one to quantify the interaction of sulfur with Ni, which can occur via chemisorption or bulk transformation of the anode by the formation of the nickel sulfide phase. It is worth mentioning that, in the past, some thermodynamic analyses were carried out to investigate the interaction between sulfur and Ni-based anodes [5,20]. These previous analyses were based on the construction of predominance area diagrams. Even though these diagrams can be used for predicting the stability of SOFC anode materials over a range of partial pressure of sulfur and oxygen, predominance area diagrams do not allow quantifying the interaction between Ni and sulfur occurring via chemisorption. In these diagrams, all the lines are two-phase boundaries, and the areas represent single phase fields. In order to explain electrochemical impedance spectroscopy (EIS) results using predominance area diagrams, Lohsoontorn et al. [5] considered the movement of the operating points relative to the phase boundary between Ni and nickel sulfide. For example, increasing H_2S concentration generates a movement upwards within the stability region of Ni, shifting the operating point to a position closer to the Ni/Ni_3S_2 phase boundary. According to these authors, this movement mirrors the trend for the H_2S to have an increasing impact on the anode as manifest through the EIS measurement. Therefore, the degree of sulfur poisoning is analyzed in a qualitative way from predominance area diagrams; that is, the closer to the Ni/Ni_3S_2 phase boundary, the stronger the interaction of sulfur with Ni catalyst. Aiming at providing a more comprehensive and quantitative analysis, thermodynamics of sulfur poisoning of Ni-based anodes is revisited in the present study. The present research aims to:

- Systematize the understanding of sulfur poisoning of Ni-based anodes through the construction of Ni–S Gibbs energy diagrams. These diagrams show the effect of operating parameters (H_2S concentration, temperature, current density and fuel utilization) on chemical potentials, nickel sulfide activity and driving force for the nickel sulfide phase formation; the present study elucidates the relationship between these thermodynamic quantities and the degree of sulfur poisoning of Ni catalyst.
- Contribute for clarifying the role of current density and fuel utilization in deactivation by sulfur; theoretical results are compared with the recent experimental findings reported by Hagen et al. [18].

It is believed that the present study in combination with our previous work [19] can provide a fairly comprehensive framework related to the sulfur poisoning of Ni-based anodes. While our previous study was focused on anode materials, the present research focuses on the effect of operating variables on sulfur poisoning of Ni-based anodes.

2. Methodology

2.1. Theoretical background

The Gibbs energy minimization method (non-stoichiometric approach) has been widely used to determine the equilibrium

compositions, as can be seen in several works [19,21,22]. The main advantage of this method is that there is no necessity of knowing the exact reactions involved. The total free energy of the system, composed of an ideal gas phase and condensed phases (pure substances, liquid or solid), may be expressed as:

$$\frac{G}{RT} = \left(\sum_{i=1}^{N} n_i \left[\frac{G_i^{\circ}}{RT} + \ln(x_i P) \right] \right)_{\text{gas}} + \frac{1}{RT} \left(\sum_{i=1}^{N} n_i G_i^{\circ} \right)_{\text{condensed}} \quad (1)$$

For the ideal gas phase, $i \in \{H_2, H_2O, CH_4, CO, CO_2, H_2S, S_2\}$; for the condensed phases, $i \in \{Ni, Ni_3S_2, C_{(graphite)}\}$.

The problem consists in finding the different values of n_i and x_i that minimize the objective function given by Eq. (1), subject to the elemental mass balance constraints, Eq. (2):

$$\sum_{i=1}^{N} n_i \delta_{ik} = b_k \quad k = 1, ..., \text{M} \quad (2)$$

When an SOFC is producing a current, there is a net input of oxygen ions (O^{2-}) to the anodic compartment that changes the equilibrium conditions of the system. Thus, moles of oxygen must be added to the elemental mass balance of oxygen (O), as shown in Eq. (3). While b_O corresponds to the moles of oxygen in the system, obtained from the inlet feed mixture at the anode, b_O^{echem} is the extra number of moles of oxygen due to the electrochemical reaction [21]:

$$\sum_{i=1}^{N} n_i \delta_{iO} = b_O + b_O^{\text{echem}} \quad (3)$$

From Faraday's Law, one can calculate the number of moles of oxygen available at the anode, considering a complete diffusion of oxygen ions from the cathode to the anode through the dense electrolyte [21]:

$$b_O^{\text{echem}} \left(\text{mol cm}^{-2}\text{s}^{-1} \right) = \frac{j}{2F} \quad (4)$$

where j is the current density in A cm^{-2} and F is Faraday's constant.

For a fuel mixture composed of CH_4, H_2 and H_2O, fuel utilization (U_f) can be calculated as follows:

$$U_f(\%) = \left(\frac{b_O^{\text{echem}}}{4n_{CH_4}^{\circ} + n_{H_2}^{\circ}} \right) \times 100 \quad (5)$$

Combining Eqs. (4) and (5), current density can be related to fuel utilization:

$$j = \frac{2F U_f(\%) \left(4n_{CH_4}^{\circ} + n_{H_2}^{\circ} \right)}{100} \quad (6)$$

Thermodynamic calculations were carried out using the *FactSage* program (version 6.3) and the *Equilib* module. The SGPS database was employed in our thermodynamic simulations. A detailed description of *Factsage* thermochemical software and databases can be seen in Refs. [23–25]. Thermodynamic analysis is carried out in the temperature range of 867–1123 K. In this way, the phase transition for nickel sulfide (Ni_3S_2), from solid to liquid at 1062 K, is considered. Besides, $P = 101.3$ kPa throughout this work.

2.2. Equilibrium sulfur coverage on Ni surface

Sulfur chemisorption on Ni surface can be described by the following equilibrium isotherm [26]:

$$\frac{pH_2S}{pH_2} = \exp\left(\frac{\Delta H_{\circ}^{\circ}(1 - \alpha\theta)}{RT} - \frac{\Delta S^{\circ}}{R} \right) \quad (7)$$

with $\Delta H_{\circ}^{\circ} = -289$ kJ mol^{-1}, $\Delta S^{\circ} = -19$ J mol^{-1} K^{-1}, and $\alpha = 0.69$. $\Delta H_{\circ}^{\circ}$ is the enthalpy of adsorption for $\theta = 0$, and ΔS° stands for the entropy of adsorption, which is independent of θ. The surface coverage θ is defined by Rostrup-Nielsen et al. [26] as the ratio between the actual (s) and the saturation (s_0) amounts of adsorbed sulfur ($\theta = s/s_0$).

The standard Gibbs energy of adsorption$\Delta G_{\text{ads}}^{\circ}$, can be written for a Temkin-like isotherm as:

$$\Delta G_{\text{ads}}^{\circ} = \Delta H_{\circ}^{\circ}(1 - \alpha\theta) - T\Delta S^{\circ} \quad (8)$$

Note that this model predicts a linear increase in the enthalpy of chemisorption as a function of coverage, through the fitting parameter α. In this way, Eq. (7) can also be written as:

$$\frac{pH_2S}{pH_2} = \exp\left(\frac{\Delta G_{\text{ads}}^{\circ}}{RT} \right) \quad (9)$$

As shown in our previous work [19], by rearranging Eq. (7), one can calculate the sulfur coverage on Ni surface as follows:

$$\theta = \frac{\frac{\Delta H_{\circ}^{\circ}}{RT} - \frac{\Delta S^{\circ}}{R} - \ln\left(\frac{pH_2S}{pH_2} \right)}{\frac{\alpha \Delta H_{\circ}^{\circ}}{RT}} \quad (10)$$

After each equilibrium calculation, the computed p_{H2S}/p_{H2} ratio can be substituted into Eq. (10), enabling one to determine the θ value.

2.3. Activity of a pure condensed phase: determination from optimization theory and stoichiometric reactions

The activity of a given species i can be related to the Lagrange's multipliers through a mathematical relationship given by Eq. (11) [27]:

$$\ln a_i = \left(\frac{-G_i^{\circ}}{RT} \right) + \sum_k \left(\frac{\lambda_k}{RT} \right) \delta_{ik} \quad (11)$$

In this work, the focus is on the activity of a chemical compound (bulk nickel sulfide). Eq. (11) is particularly useful whenever the equilibrium state is determined by a minimization algorithm. In this case, activity is readily calculated from Lagrange's multipliers even for complex multiphase multicomponent systems. Thermochemical softwares, such as *FactSage*, which apply the Gibbs energy minimization method, normally provide to the user, after the completion of equilibrium computation, activity values for all the phases, besides the number of moles and molar fraction of the mixture constituents [19]. In the present study, the graphical meaning of chemical potentials, activity and Lagrange's multipliers will be widely explored through the construction of the Ni–S Gibbs energy diagram.

The generic stoichiometric reaction (R1) for the bulk nickel sulfide formation is described as follows:

$$(y/z)Ni_{(s)} + H_2S_{(g)} \leftrightarrow (1/z)Ni_yS_z + H_{2(g)} \quad (R1)$$

The bulk nickel sulfide can exist at the solid or liquid state, depending on the temperature. For pure Ni, $a_{Ni} = 1$. From stoichiometric approach, nickel sulfide activity can be determined as follows:

$$a_{Ni_ySz} = \left[\left(\frac{pH_2S}{pH_2}\right)\cdot K_{Ni_ySz,bulk}\right]^z \quad (12)$$

with $K_{Ni_ySz,bulk} = \exp(-\Delta G^{\circ}_{Ni_ySz,bulk}/RT)$. $\Delta G^{\circ}_{Ni_ySz,bulk}$ corresponds to the standard Gibbs energy of formation of nickel sulfide.

2.4. Nickel sulfide activity and driving force for nickel sulfide formation as a function of sulfur coverage on Ni surface

By combining Eqs. (9) and (12), the activity of the nickel sulfide phase can be mathematically expressed as a function of the difference between the values of ΔG°_{ads} and $\Delta G^{\circ}_{Ni_ySz,bulk}$ [19]:

$$a_{Ni_ySz} = \left(\exp\left(\frac{\Delta G^{\circ}_{ads} - \Delta G^{\circ}_{Ni_ySz,bulk}}{RT}\right)\right)^z \quad (13)$$

Remembering that

$$\Delta\mu_{Ni_ySz} = RT\ln a_{Ni_ySz} \quad (14)$$

and that the driving force for the formation of a bulk phase is essentially a difference in chemical potentials [28], one can see that $D_{NiySz} \equiv \Delta\mu_{NiySz}$, where D_{NiySz} is the driving force for the formation of the nickel sulfide phase. In this way, Eq. (14) can be rewritten as:

$$a_{Ni_ySz} = \exp\left(\frac{D_{Ni_ySz}}{RT}\right) \quad (15)$$

By combining Eqs. (13) and (15), the following relationship is obtained:

$$D_{Ni_ySz} = z\cdot\left(\Delta G^{\circ}_{ads} - \Delta G^{\circ}_{Ni_ySz,bulk}\right) \quad (16)$$

One can see from Eqs. (13) and (16) that nickel sulfide activity and driving force for nickel sulfide formation become a function of θ; this fact can be ascribed to the dependence of ΔG°_{ads} on θ, as shown in Eq. (8). Typically, activity and driving force are thermodynamic quantities that measure the thermodynamic instability of a certain phase. When the activity of the nickel sulfide phase is equal to unity, one can see from Eq. (14) that $\Delta\mu_{NiySz} = 0$ and, thus, $D_{NiySz} = 0$. In this case, the bulk nickel sulfide phase is thermodynamically stable [29,30]; on the other hand, Eq. (14) shows that $D_{NiySz} < 0$ when $a_{NiySz} < 1$. Consequently, the nickel sulfide phase is thermodynamically unstable. The negative value computed for D_{NiySz} corresponds to the amount of Gibbs energy that would have to be added to the phase to make it stable if all other conditions remained unchanged [29]. For values of nickel sulfide activity increasingly lower than unity, D_{NiySz} becomes increasingly negative; as a result, the bulk nickel sulfide phase becomes increasingly unstable [30]. From Eqs. (13) and (16), one can verify that the bulk nickel sulfide phase is thermodynamically stable ($a_{NiySz} = 1$ and $D_{NiySz} = 0$) when $\Delta G^{\circ}_{ads} = \Delta G^{\circ}_{Ni_ySz,bulk}$; on the other hand, the bulk nickel sulfide phase is unstable and cannot be formed under the equilibrium conditions ($a_{NiySz} < 1$ and $D_{NiySz} < 0$) when $\Delta G^{\circ}_{ads} < \Delta G^{\circ}_{Ni_ySz,bulk}$. Fig. 1 illustrates, for the nickel sulfide phase Ni_3S_2, at 830 K, the dependence of $a_{Ni_3S_2}$, $D_{Ni_3S_2}$ and ΔG°_{ads} on θ. As θ increases, ΔG°_{ads} also increases; at a sufficiently high value of θ (1.13, in this example), ΔG°_{ads} equals $\Delta G^{\circ}_{Ni_3S_2,bulk}$, resulting in the formation of the nickel sulfide phase Ni_3S_2 ($a_{Ni_3S_2} = 1$ and $D_{Ni_3S_2} = 0$). For θ values lower than 1.13, nickel sulfide phase is unstable ($a_{Ni_3S_2} < 1$ and $D_{Ni_3S_2} < 0$); in this case, the interaction of sulfur with Ni occurs via chemisorption. As illustrated in Fig. 1(a), nickel sulfide activity and driving force for nickel sulfide formation are strictly increasing functions of θ; therefore, as the degree of sulfur coverage increases,

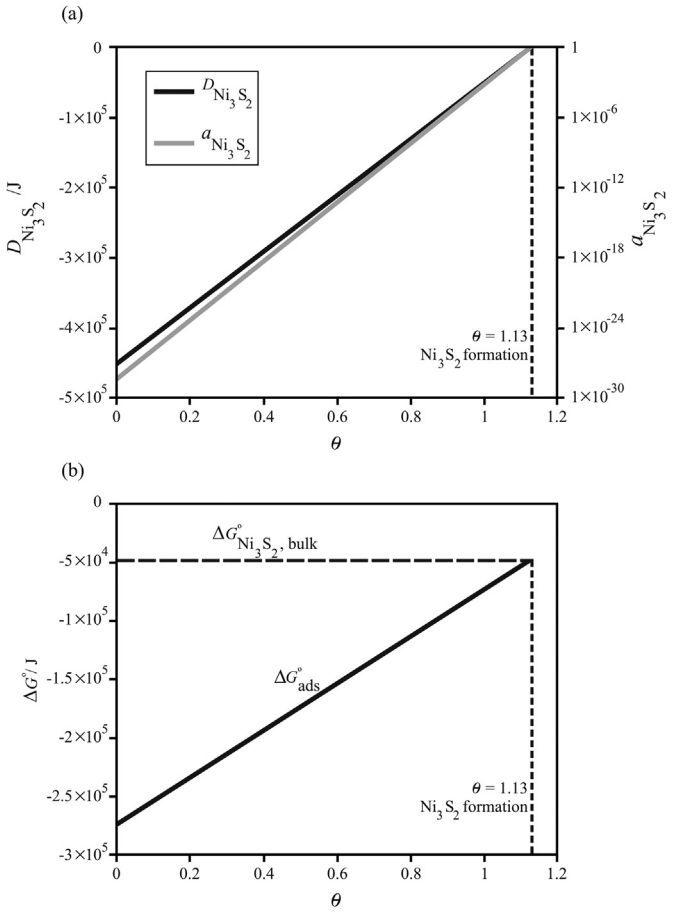

Fig. 1. (**a**) Driving force for nickel sulfide formation and nickel sulfide activity as a function of sulfur coverage on Ni surface. (**b**) ΔG°_{ads} and $\Delta G^{\circ}_{Ni_3S_2,bulk}$ as a function of sulfur coverage on Ni surface. $T = 830$ K.

the nickel sulfide activity also increases. This fact is noteworthy, because, even under conditions where the nickel sulfide phase is unstable, the nickel sulfide activity can quantify the interaction between Ni and sulfur that occurs via chemisorption. Thus, the increase in nickel sulfide activity corresponds to a stronger interaction between Ni and sulfur, due to a higher degree of sulfur coverage on nickel active sites; as consequence, fewer sites are available for catalysis, which leads to an increase in the cell performance loss. In this way, thermodynamic analysis based on nickel sulfide activity allows one to evaluate the interaction between Ni and sulfur that occurs via chemisorption ($a_{NiySz} < 1$) or via bulk transformation of the anode by the formation of the nickel sulfide phase ($a_{NiySz} = 1$). According to previous works [3,4,18,31,32], the interaction of sulfur impurities with Ni-based anodes occurs by adsorption/chemisorption at active sites of Ni catalyst or by the formation of the bulk nickel sulfide phase. Thus, the study based on nickel sulfide activity is suitable for the investigation of the sulfur poisoning behavior.

2.5. Ni–S Gibbs energy diagram and the graphical determination of the nickel sulfide activity

In this section, the basic principles involved in the construction of the Ni–S Gibbs energy diagram are discussed. This diagram is of great relevance because it shows that the sulfur chemical potential (μ_S) controls the nickel sulfide activity. Fig. 2(a) and (b) depicts a schematic representation of the Ni–S Gibbs energy diagram at a

fixed temperature. In Fig. 2(b), the sulfur chemical potential is high enough to induce the formation of the bulk nickel sulfide phase. On the other hand, as shown in Fig. 2(a), the sulfur chemical potential is much lower, and, in this case, the formation of the bulk nickel sulfide phase does not occur. The detailed explanation is provided in the next paragraphs.

After determining the equilibrium partial pressure of S_2, the value of μ_S can be readily calculated as follows:

$$\mu_S = 0.5\mu^{\circ}_{S_2} + RT \ln p_{S_2}^{0.5} \tag{17}$$

The standard chemical potentials of pure Ni (μ°_{Ni}), nickel sulfide ($\mu^{\circ}_{Ni_yS_z}$) and sulfur ($\mu^{\circ}_{S} = 0.5\mu^{\circ}_{S_2}$) are fixed at a given temperature. As shown in Fig. 2(a), the value of $\frac{1}{(y+z)}\mu^{\circ}_{Ni_yS_z}$ is represented by a circle. Note also that the values of μ°_{Ni} and μ_S determine a straight line in the Ni–S Gibbs energy diagram. The distance between this line and the circle corresponds to the value of $|\Delta\bar{\mu}|$ [19]:

$$\Delta\bar{\mu} = \frac{1}{(y+z)}\mu_{Ni_yS_z} - \frac{1}{(y+z)}\mu^{\circ}_{Ni_yS_z} = \frac{\Delta\mu_{Ni_yS_z}}{(y+z)}, \Delta\bar{\mu} < 0 \tag{18}$$

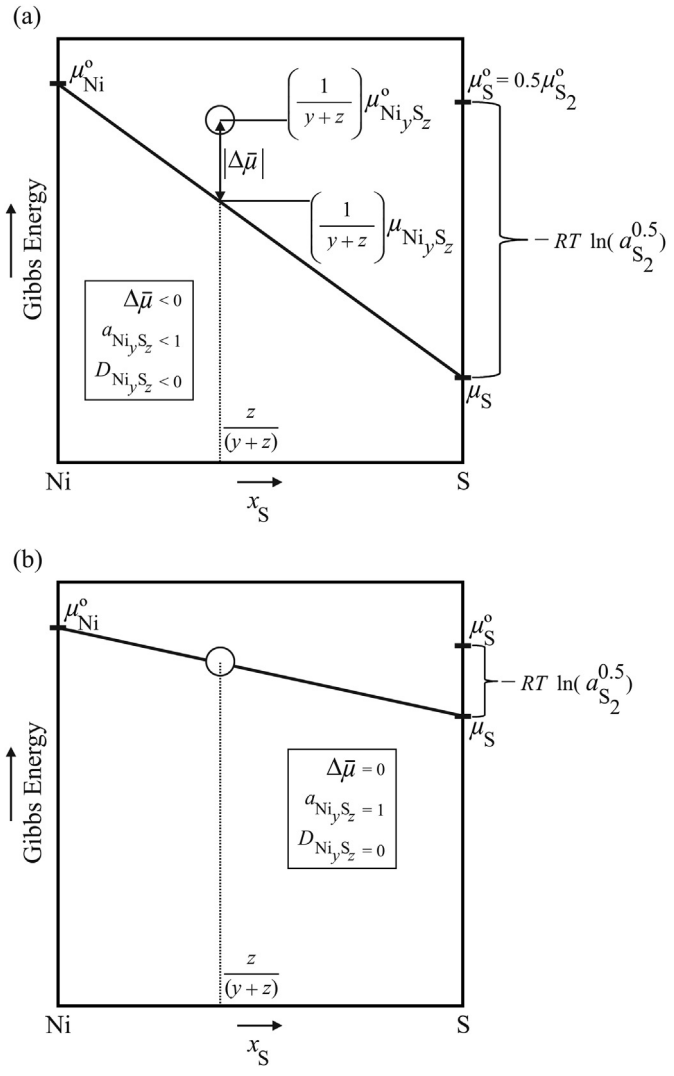

Fig. 2. Schematic representation of Ni–S Gibbs energy diagram at a fixed temperature, for two cases: (**a**) bulk nickel sulfide phase Ni_yS_z is thermodynamically unstable, and (**b**) bulk phase Ni_yS_z is thermodynamically stable under equilibrium conditions. $a_{S_2} = p_{S_2}/P^{\circ}$, where P° corresponds to the standard-state pressure (101.3 kPa).

Note that $|\Delta\bar{\mu}|$ is evaluated at $x_S = z/(y+z)$. The value of $1/(y+z)$ μ_{NiySz} belongs to the straight line that connects μ°_{Ni} withμ_S. In this way, this term can be calculated by Eq. (19):

$$\frac{1}{(y+z)}\mu_{Ni_yS_z} = x_S\mu_S + (1-x_S)\mu^{\circ}_{Ni} \tag{19}$$

Combining Eqs. (14) and (18), the activity of Ni_yS_z can be determined as follows:

$$a_{Ni_yS_z} = \exp\left(\frac{(y+z)\Delta\bar{\mu}}{RT}\right) \tag{20}$$

In Fig. 2(a), the sulfur chemical potential is very low; thus, the straight line connecting μ°_{Ni} withμ_S passes below the circle. Since $\Delta\bar{\mu} < 0$, one can verify from Eq. (20) that $a_{NiySz} < 1$ (nickel sulfide phase is thermodynamically unstable). In Fig. 2(b), μ_S is so high that it causes the straight line connecting μ°_{Ni} and μ_S to cross the circle; thus, $\Delta\bar{\mu} = 0$. In this case, one obtains from Eq. (20) that $a_{NiySz} = 1$, which indicates that nickel sulfide phase is thermodynamically stable. Since a constant temperature is assumed in our schematic representation, one can state that the increase in μ_S results from the increase inp_{S2}. Interestingly, one can see from Eq. (11) that, for an elemental species, the Lagrange's multiplier corresponds to the chemical potential, with $\delta_{ik} = 1$. In this way, $\lambda_S = \mu_S$ and $\lambda_{Ni} = \mu^{\circ}_{Ni}$. It is worthwhile highlighting the relevance of Eq. (11), which correlates Lagrange's multipliers, from mathematical optimization, to chemical potentials, allowing representing Lagrange's multipliers in a Gibbs energy diagram.

It is worth noting that the nickel sulfide activity can be determined by means of the graphical analysis applied to the Ni–S Gibbs energy diagram, as explained in this section, or directly through other methods, such as the sensitivity analysis from the optimization theory (Eq. (11)) or stoichiometric reaction (R1). Independently of the method, the values are essentially the same; however, the graphical determination from the Ni–S Gibbs energy diagram is advantageous because it allows one to see how the sulfur chemical potential controls the nickel sulfide activity, and, as a consequence, the driving force for the formation of the nickel sulfide phase. The proposed diagram allows observing the effect of different operating variables (H_2S concentration, temperature, fuel composition, current density and fuel utilization) on μ_S. In the next sections, the nickel sulfide activity analysis is focused on the phase Ni_3S_2. Other nickel sulfides could have also been considered in this study (*e.g.*, NiS, Ni_3S_4, Ni_6S_5, NiS_2).

3. Results and discussion

3.1. Effect of H_2S concentration and temperature on the degree of sulfur interaction with Ni for hydrogen-fueled SOFC

The Ni–S Gibbs energy diagram from Fig. 3 shows the effect of H_2S concentration (1, 100 and 1300 ppm) on sulfur chemical potential for an SOFC operating on a mixture of hydrogen and steam (97% H_2, 3% H_2O) at 867 K. The line corresponding to the H_2S concentration of 3 ppm (Case II) was not shown in order to ensure a better clarity of the graphical representation. All numerical data are provided in the table presented together with the diagram. As H_2S concentration in the inlet gas is increased from 1 to 100 ppm, the value of $|\Delta\bar{\mu}|$ decreases due to the increase inμ_S; as a consequence, nickel sulfide activity and driving force for the formation of the Ni_3S_2 phase become greater, suggesting a stronger interaction between Ni and sulfur. At 1300 ppm, μ_S is high enough to ensure the formation of the bulk Ni_3S_2 phase – in this case, $|\Delta\bar{\mu}| = 0$, which results in $a_{Ni_3S_2} = 1$ and $D_{Ni_3S_2} = 0$. The value of θ also increases with increasing H_2S concentration. In theory, the poisoning of Ni catalyst

Case	[H_2S], ppm	$\lvert\Delta\bar{\mu}\rvert$, J	μ_S, J	p_{S_2}, kPa	$a_{Ni_3S_2}$	$D_{Ni_3S_2}$, J	θ	ΔR_p, Ωcm^2[5]
I	1	2.06×10^{4}	-1.88×10^{5}	1.9×10^{-16}	6.3×10^{-7}	-1.03×10^{5}	0.87	1.4
II	3	1.74×10^{4}	-1.80×10^{5}	1.7×10^{-15}	5.7×10^{-6}	-8.70×10^{4}	0.91	4.8
III	100	7.30×10^{3}	-1.55×10^{5}	1.9×10^{-12}	6.3×10^{-3}	-3.65×10^{4}	1.03	n/a
IV	1300	0	-1.36×10^{5}	3.0×10^{-10}	1	0	1.13	n/a

n/a:not available in Ref. [5]

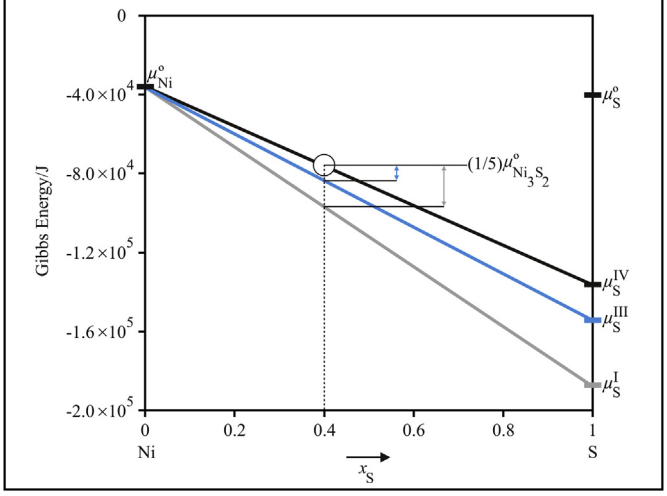

Fig. 3. Ni–S Gibbs energy diagram showing the effect of H_2S concentration on sulfur chemical potentials for the cases I, III and IV. Relevant numerical data are provided along with the diagram. Fuel: wet hydrogen (97% H_2 + 3%H_2O). T = 867 K. The length of the arrow (↕) represents the value of $|\Delta\bar{\mu}|$; the gray and blue arrows correspond to the cases I and III, respectively. (For interpretation of the references to colour in this figure legend, the reader is referred to the web version of this article.)

Case	T, K	$\lvert\Delta\bar{\mu}\rvert$, J	μ_S, J	p_{S_2}, kPa	$a_{Ni_3S_2}$	$D_{Ni_3S_2}$, J	θ	ΔR_p, Ωcm^2[5]
I	830	1.88×10^{4}	-1.80×10^{5}	6.4×10^{-17}	1.2×10^{-6}	-9.41×10^{4}	0.89	4.8
II	873	2.09×10^{4}	-1.89×10^{5}	2.3×10^{-16}	5.7×10^{-7}	-1.04×10^{5}	0.86	1.4
III	1273	3.80×10^{4}	-2.70×10^{5}	5.6×10^{-13}	1.6×10^{-8}	-1.90×10^{5}	0.60	n/a

n/a:not available in Ref. [5]

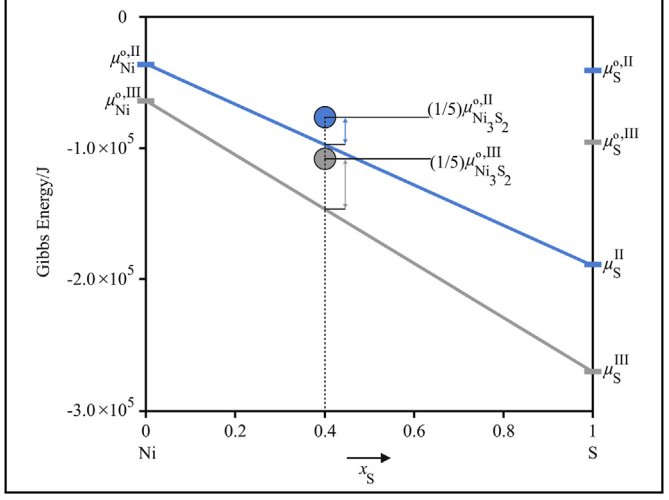

Fig. 4. Ni–S Gibbs energy diagram showing the effect of temperature on standard chemical potentials and sulfur chemical potentials for the cases II and III. Relevant numerical data are provided along with the diagram. Fuel: wet hydrogen (97% H_2 + 3% H_2O) containing 1 ppm H_2S. The length of the arrow (↕) represents the value of $|\Delta\bar{\mu}|$; the blue and gray arrows correspond to the cases II and III, respectively. (For interpretation of the references to colour in this figure legend, the reader is referred to the web version of this article.)

will be greater at higher values of θ, due to a lower availability of sites for electro-catalysis. Thus, it is expected that the performance loss increases with the increase in the value of θ. In fact, by raising the H_2S content from 1 to 3 ppm, Lohsoontorn et al. [5] experimentally verified that the extent of the polarization impedance (ΔR_p) increased from 1.4 to 4.8 Ωcm^2, which is consistent with the increase in the θ value from 0.87 to 0.91. Note that at θ = 1.13, the bulk nickel sulfide phase Ni_3S_2 can be formed. Based on θ definition, one could infer that when the actual amount of adsorbed sulfur is 13% greater than the sulfur saturation, the nucleation of Ni_3S_2 phase occurs at 867 K in wet hydrogen atmosphere. It is worth pointing out that, depending on the value of sulfur chemical potential, the interaction between sulfur and Ni can occur via chemisorption (cases I, II and III) or bulk transformation by the formation of the new phase Ni_3S_2 (case IV).

The Ni–S Gibbs energy diagram in Fig. 4 shows the effect of temperature on chemical potentials for an SOFC operating on wet hydrogen (97%H_2, 3%H_2O) containing 1 ppm H_2S. As shown in the diagram, the reduction of the operating temperature of SOFC increases μ_S, leading to a decrease in the value of $|\Delta\bar{\mu}|$, which results in an increase in the nickel sulfide activity. Reducing operating temperature affects mostly μ_S; the standard chemical potentials of Ni and Ni_3S_2 are only slightly increased with decrease in temperature. In this way, the interaction between Ni and sulfur is stronger at lower temperatures mainly due to the remarkable increase in the μ_S value. The value of θ increases as the operating temperature is reduced, which is in agreement with the increase in the polarization impedance reported by Lohsoontorn et al. [5] (cases I and II). It is also worth noting that, unlike $a_{Ni_3S_2}$, p_{S2} decreases as temperature is lowered. Actually, p_{S2} follows the same trend as $a_{Ni_3S_2}$ only when temperature is held constant (see Figs. 3 and 6). Therefore, the partial pressure of S_2 should not be used alone to quantify the degree of sulfur poisoning of Ni catalyst; the interaction of sulfur with Ni should be quantified by nickel sulfide activity or θ.

Fig. 5 depicts the effect of H_2S concentration and temperature on nickel sulfide activity (**a**), driving force for nickel sulfide formation (**b**), θ (**c**) and experimental values of relative power output drop, ΔW_r ($\Delta W_r = (W - W^s)/W$, in which W and W^s are power output before and after initial quick sulfur poisoning, respectively) (**d**). As one can see, the experimental and simulation values exhibit similar trends: at a fixed temperature, they increase first rapidly, for H_2S concentrations lower than 1 ppm, and then gradually as H_2S concentration is increased from 1 to 10 ppm. Note that, in all the cases, the curves are moved upwards with decrease in temperature, indicating that the sulfur poisoning effect is more pronounced at lower temperatures.

3.2. *Effect of H_2S concentration and current density on the degree of sulfur interaction with Ni for methane-fueled SOFC*

The Ni–S Gibbs energy diagram in Fig. 6 shows that, for an SOFC operating on methane fuel (29% CH_4, 58% H_2O and 13%H_2) containing 20 ppm H_2S, at 1123 K, the increase in current density leads to an increase in μ_S and hence in $a_{Ni_3S_2}$. Increasing current density means that a higher influx of oxide ions (O^{2-}) is made available at the anode; in this way, μ_S increases as a result of the increase in p_{S2}. Interestingly, when current density is increased to 1 A cm^{-2}, nickel sulfide activity reaches its maximum value, indicating a bulk transformation by the formation of the nickel sulfide phase. Thus, even at a relatively high temperature and at very low H_2S concentration, the formation of Ni_3S_2 phase occurs due to the increase in current density. This fact is noteworthy, because it is normally accepted that the formation of the nickel sulfide phase requires very high sulfur concentrations and low operating temperatures [3]. Indeed, as previously shown in Fig. 3, the formation of the bulk phase Ni_3S_2 requires a very high H_2S concentration (1300 ppm) at a

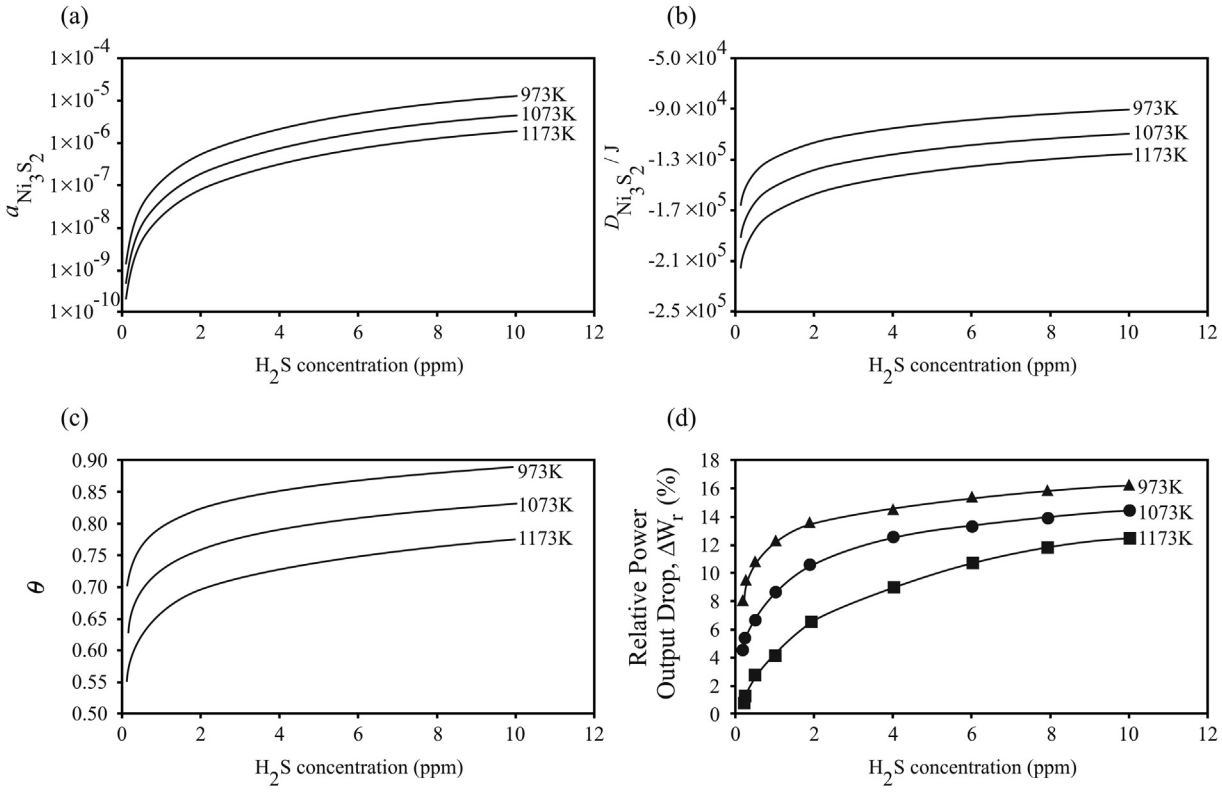

Fig. 5. Simulated values of $a_{Ni_3S_2}$ (**a**), $D_{Ni_3S_2}$ (**b**) and θ (**c**) as a function of H_2S concentration, for $T = 973$, 1073 and 1173 K. Experimental values reported by Zha et al. [4] for relative power output drop as a function of H_2S concentration, for $T = 973$, 1073 and 1173 K (**d**). Fuel: $H_2 + H_2S$ mixture.

Case	j, A·cm^{-2}	U_f(%)	$\lvert\Delta\bar{\mu}\rvert$, J	μ_S, J	p_{S_2}, kPa	$a_{Ni_3S_2}$	$D_{Ni_3S_2}$, J	θ
I	0 (OCV)	0	2.12×10^{4}	-2.12×10^{5}	1.9×10^{-11}	1.2×10^{-5}	-1.06×10^{5}	0.83
II	0.5	49.8	1.86×10^{4}	-2.06×10^{5}	7.7×10^{-11}	4.8×10^{-5}	-9.28×10^{4}	0.87
III	1	99.6	0	-1.59×10^{5}	1.6×10^{-6}	1	0	1.1

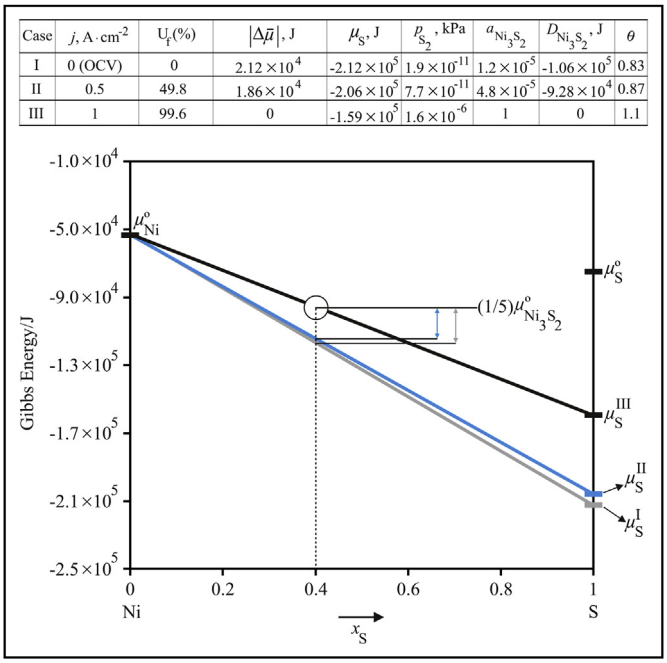

Fig. 6. Ni–S Gibbs energy diagram showing the effect of current density and fuel utilization on sulfur chemical potentials for the cases I, II and III. Relevant numerical data are provided along with the diagram. Inlet H_2S concentration: 20 ppm. Anode inlet condition: $n^{\circ}_{CH_4} = 1.17\times10^{-6}$, $n^{\circ}_{H_2O} = 2.34\times10^{-6}$ and $n^{\circ}_{H_2} = 5.24\times10^{-7}$ [mol cm^{-2} s^{-1}]. $T = 1123$ K. The length of the arrow (↕) represents the value of $|\Delta\bar{\mu}|$; the gray and blue arrows correspond to the cases I and II, respectively. (For interpretation of the references to colour in this figure legend, the reader is referred to the web version of this article.)

relatively low operating temperature (867 K). From the results shown in Fig. 6, one can see that, when the current density is increased to 1 A cm^{-2}, μ_S becomes high enough to promote the formation of the bulk nickel sulfide phase Ni_3S_2; in this case, $|\Delta\bar{\mu}| = 0$ and $a_{Ni_3S_2} = 1$. On the other hand, the value of $|\Delta\bar{\mu}|$ decreases only slightly as a result of the increase in current density from 0 (OCV) to 0.5 A cm^{-2}; consequently, nickel sulfide activity also increases moderately. It is worth noting that the fuel utilization at 1 A cm^{-2} is nearly 100%, suggesting that high values of fuel utilization strongly enhance the interaction between Ni and sulfur. In our simulations, the inlet molar flow rate was selected in such a way that the fuel utilization was approximately 100% at the current density of 1 A cm^{-2} (see Figs. 6 and **7**). Fig. 7 shows that as fuel utilization increases, H_2 and CO are consumed by the electrochemical reactions producing H_2O and CO_2. Nickel sulfide activity increases first gradually for fuel utilizations lower than 90%, and, then, very steeply as fuel utilization is increased from 90 to 100%. In this way, under fuel starvation conditions (very low concentrations of H_2 and CO due to high fuel utilizations), nickel sulfide activity is greatly increased, indicating a strong interaction between Ni and sulfur, which can lead to severe deactivation of Ni. As expected, the values of θ follow the same trend as the nickel sulfide activity. When fuel utilization is approximately 100%, nickel sulfide activity becomes equal to unity, and the formation of the bulk Ni_3S_2 phase is feasible; under these conditions, the θ value is 1.1, which means that, at a super-saturation of adsorbed sulfur of 10%, the nucleation of the Ni_3S_2 phase may occur. From the results shown in Figs. 6 and 7, one can see that the increase in current density and fuel utilization does not alleviate the sulfur poisoning of Ni catalyst; on the contrary, when fuel utilization increases, a greater degree of anode degradation should be expected, due to the enhanced interaction between Ni and sulfur. In addition, the results show that the effect

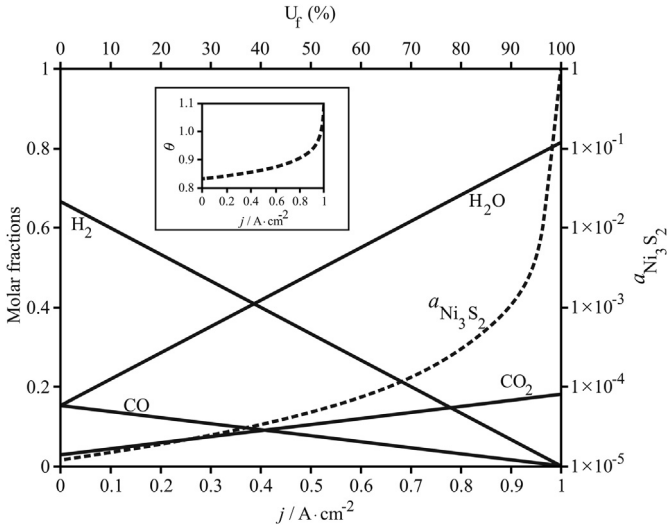

Fig. 7. Molar fraction of species (H_2, H_2O, CO, CO_2), nickel sulfide activity and sulfur coverage on Ni surface as a function of current density and fuel utilization. Inlet H_2S concentration: 20 ppm. Anode inlet condition: $n^{\circ}_{CH_4} = 1.17 \times 10^{-6}$, $n^{\circ}_{H_2O} = 2.34 \times 10^{-6}$ and $n^{\circ}_{H_2} = 5.24 \times 10^{-7}$ [mol cm^{-2} s^{-1}]. $T = 1123$ K.

of current density on the degree of sulfur poisoning (quantified by the values of θ and $a_{Ni_3S_2}$) becomes noteworthy when fuel utilization approaches 100% (fuel starvation conditions). These thermodynamic findings can be closely related to the recent experimental results reported by Hagen et al. [18]. At current densities up to 0.5 A cm^{-2}, these authors observed only moderate cell performance losses; at 1 A cm^{-2}, however, they observed very large cell voltage drops. According to Hagen et al. [18], it is likely that fuel utilization close to 100% has been achieved during the operation at 1 A cm^{-2}; based on this possibility, they concluded that deactivation by sulfur is more severe under conditions where fuel starvation is highly likely. Fig. 8 shows the results obtained from thermodynamic analysis ($a_{Ni_3S_2}$, $D_{Ni_3S_2}$ and θ) along with the experimental values of voltage drop reported by Hagen et al. [18]. As one can see, the experimental and simulation values exhibit similar trends: at a fixed current density, they increase with the increase in H_2S; for OCV, 0.25 and 0.5 A cm^{-2}, both theoretical and experimental curves tend to level off for higher H_2S concentrations (a similar behavior was also observed in Fig. 5). It is worth noting that, while the theoretical curves are very close to each other for current densities in the range of 0 (OCV) to 0.5 A cm^{-2}, at 1 A cm^{-2}, the theoretical curve is well above the other curves. For example, Fig. 8(a) shows that, at 10 ppm H_2S, nickel sulfide activity is slightly increased from

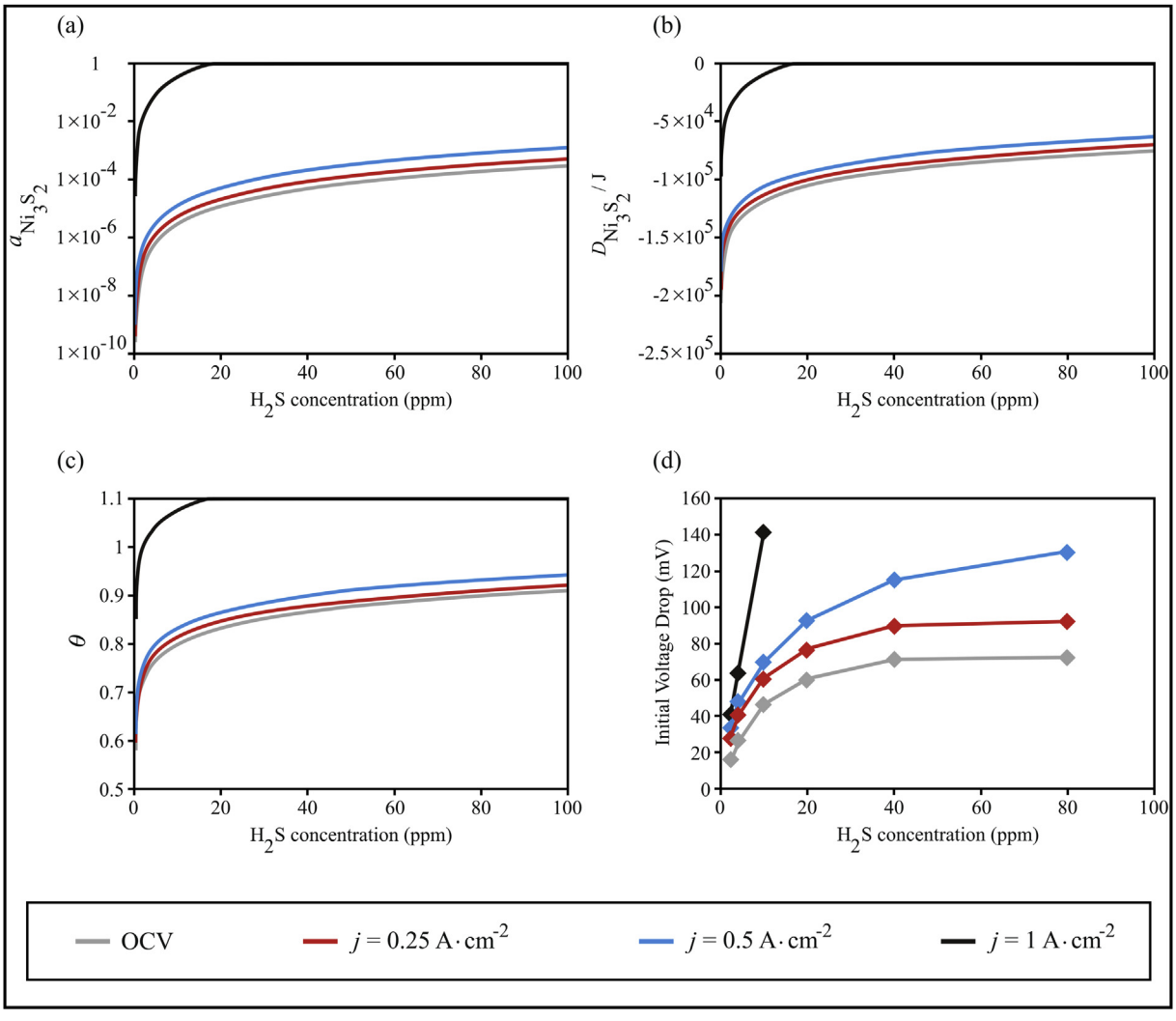

Fig. 8. Simulated values of $a_{Ni_3S_2}$ (**a**), $D_{Ni_3S_2}$ (**b**) and θ (**c**) as a function of H_2S concentration, for $j = 0$ A cm^{-2} (OCV, $U_f = 0\%$), 0.25 A cm^{-2} ($U_f = 24.9\%$), 0.5 A cm^{-2} ($U_f = 49.8\%$) and 1 A cm^{-2} ($U_f = 99.6\%$). Experimental values reported by Hagen et al. [18] for initial voltage drop as a function of H_2S concentration, for $j = 0$, 0.25, 0.5 and 1 A cm^{-2} (**d**). Simulation conditions: $n^{\circ}_{CH_4} = 1.17 \times 10^{-6}$, $n^{\circ}_{H_2O} = 2.34 \times 10^{-6}$ and $n^{\circ}_{H_2} = 5.24 \times 10^{-7}$ [mol cm^{-2} s^{-1}]. $T = 1123$ K.

3.0×10^{-6} to 1.2×10^{-5} when current density is increased from 0 (OCV) to 0.5 A cm^{-2}; however, a further increase in the current density to 1 A cm^{-2} results in a dramatic increase in the value of nickel sulfide activity to 0.3. Thus, it is noteworthy that, at a fixed inlet H_2S concentration, nickel sulfide activity can be increased 25.000 times due only to the increase in current density from 0.5 to 1 A cm^{-2}. In this way, since the interaction between Ni and sulfur is maximized at 1 A cm^{-2}, deactivation by sulfur must be much greater under this condition. In fact, Fig. 8(d) shows that, at 10 ppm H_2S, the voltage drop moderately increases from 40 to 70 mV due to the increase in current density from 0 (OCV) to 0.5 A cm^{-2} (note that the curves are also very close to each other); however, at 1 A cm^{-2}, the voltage drop steeply increases to 140 mV, indicating severe deactivation by sulfur. A further increase to 20 ppm H_2S during the experiments at 1 A cm^{-2} would lead to a voltage drop even greater, possibly resulting in irreversible performance losses owing to the formation of Ni_3S_2 phase. It is known that the effect of sulfur poisoning is reversible (or fully recoverable) when the interaction between nickel and sulfur occurs via adsorption/chemisorption (that is, before Ni is converted to nickel sulfide phase Ni_3S_2) [32]. Fig. 8(a)–(c) show that, in the range of 20–100 ppm H_2S, nickel sulfide phase is stable ($a_{Ni_3S_2} = 1, D_{Ni_3S_2} = 0$ and $\theta = 1.1$).

It is worth pointing out that our thermodynamic results are also corroborated by the experimental findings reported by Xia and Birss [10]. These authors verified that anode degradation is enhanced when exposure to H_2S occurs under a load and the higher the current density, the more rapid the loss of performance.

It is also worth mentioning that the ceramic phase of the anode may influence the interaction between Ni and H_2S [32]. In our previous work [19], for example, it was found that the formation of other sulfides, such as Ce_2O_2S, decreases the value of nickel sulfide activity and hence the degree of interaction of sulfur with nickel; in addition, it was shown that Ce_2O_2S can be regenerated to CeO_2 by means of the reaction with O^{2-} ions. In this way, thermodynamics show that the presence of oxide phase CeO_2 in the anode could alleviate the sulfur poisoning of Ni catalyst, which is in agreement with experimental works [33–35]. Thus, the sulfur poisoning behavior of Ni-based anodes is closely related to the degree of interaction of sulfur with Ni; by comparing theoretical results with the experimental trends reported in literature, one can see that whenever nickel sulfide activity decreases, deactivation by sulfur also decreases. In the present work, the analysis was focused on the effect of operating parameters (H_2S concentration, temperature, current density and fuel utilization) on the degree of interaction of sulfur with Ni; in this way, the interaction between the ceramic phase and sulfur was not considered. The study of the effect of the operating parameters on sulfur chemical potential and nickel sulfide activity allows one to understand and interpret experimental results reported in literature.

4. Conclusions

Ni–S Gibbs energy diagram rationalizes, in a systematic way, experimental observations related to sulfur poisoning of Ni-based SOFC anodes. This diagram shows that the degree of sulfur poisoning of Ni is indeed controlled by the sulfur chemical potential: nickel sulfide activity, which is a strictly increasing function of sulfur coverage on Ni surface, increases as the sulfur chemical potential becomes less negative. Since the fuel cell performance loss is directly related to the degree of sulfur coverage on nickel active sites, it is evident that, whenever a change in the operating condition leads to an increase in the value of the sulfur chemical potential, deactivation by sulfur is expected to be greater. It is found that sulfur chemical potential increases when H_2S concentration in fuel increases and temperature decreases, indicating that the interaction between Ni and sulfur is enhanced under these conditions, which is in agreement with several experimental studies. When H_2S concentration and temperature are held constant, an increase in current density leads to a higher sulfur chemical potential. Thus, deactivation by sulfur also becomes greater as current density increases. At fuel utilizations lower than 90%, the increase in current density modestly increases the degree of sulfur interaction with Ni. The effect of current density becomes, however, noteworthy at fuel utilizations close to 100%, when the system is composed essentially of H_2O and CO_2 (fuel starvation conditions); in this case, the interaction between Ni and sulfur is so strong that bulk nickel sulfide phase Ni_3S_2 can be formed even at very low contents of H_2S (around 20 ppm) at the relatively high temperature of 1123 K. The present results are in agreement with the recent experimental evidences related to the detrimental effect of current density during sulfur poisoning. In this way, thermodynamic analysis contributes to the understanding of the effect of different operating parameters on deactivation by sulfur.

Acknowledgments

The authors would like to thank FAPERGS (Fundação de Amparo à Pesquisa do Estado do Rio Grande do Sul) and CAPES (Coordenação de Aperfeiçoamento de Pessoal de Nível Superior) for their financial support (Postdoctoral fellowship – Edital 09/2012 – DOCFIX). Grant numbers (SPI 2842-25.51/12-0 and FPE 161/2011).

References

[1] G. Postole, F. Bosselet, G. Bergeret, S. Prakash, P. Gélin, J. Catal. 316 (2014) 149–163.
[2] A. Hagen, J.F.B. Rasmussen, K. Thydénn, J. Power Sources 196 (2011) 7271–7276.
[3] Z. Cheng, J.H. Wang, Y.M. Choi, L. Yang, M.C. Lin, M. Liu, Energy Environ. Sci. 4 (2011) 4380–4409.
[4] S. Zha, Z. Cheng, M. Liu, J. Electrochem. Soc. 154 (2007) B201–B206.
[5] P. Lohsoontorn, D.J.L. Brett, N.P. Brandon, J. Power Sources 183 (2008) 232–239.
[6] Z. Cheng, S. Zha, M. Liu, J. Power Sources 172 (2007) 688–693.
[7] Y. Matsuzaki, I. Yasuda, Solid State Ionics 132 (2000) 261–269.
[8] J.F.B. Rasmussen, A. Hagen, J. Power Sources 191 (2009) 534–541.
[9] K. Sasaki, K. Susuki, A. Iyoshi, M. Uchimura, N. Imamura, H. Kusaba, Y. Teraoka, H. Fuchino, K. Tsujimoto, Y. Uchida, N. Jingo, J. Electrochem. Soc. 153 (2006) A2023–A2029.
[10] S.J. Xia, V.I. Birss, ECS Trans. 2005–07 (2005) 1275–1283.
[11] J.F.B. Rasmussen, A. Hagen, Fuel Cells 10 (2010) 1135–1142.
[12] T.R. Smith, A. Wood, V.I. Birss, Appl. Catal. A 354 (2009) 1–7.
[13] Y. Shiratori, T. Ijichi, T. Oshima, K. Sasaki, Int. J. Hydrogen Energy 35 (2010) 7905–7912.
[14] C. Xu, J.W. Zondlo, M. Gong, F. Elizalde-Blancas, X. Liu, I.B. Celik, J. Power Sources 195 (2010) 4583–4592.
[15] E. Brightman, D.G. Ivey, D.J.L. Brett, N.P. Brandon, J. Power Sources 196 (2011) 7182–7187.
[16] D.S. Monder, K. Karan, ECS Trans. 35 (2011) 977–985.
[17] J.B. Hansen, Electrochem. Solid-State Lett. 11 (2008) B178–B180.
[18] A. Hagen, G.B. Johnson, P. Hjalmarsson, J. Power Sources 272 (2014) 776–785.
[19] A. Lima da Silva, N.C. Heck, Int. J. Hydrogen Energy 40 (2015) 2334–2353.
[20] P. Lohsoontorn, D.J.L. Brett, N.P. Brandon, J. Power Sources 175 (2008) 60–67.
[21] A. Lima da Silva, I.L. Müller, J. Power Sources 195 (2010) 5637–5644.
[22] S. Goicoechea, H. Ehrich, P.L. Arias, N. Kockmann, J. Power Sources 279 (2015) 312–322.
[23] C.W. Bale, P. Chartrand, S.A. Decterov, G. Eriksson, K. Hack, R.B. Mahfoud, et al., Calphad 26 (2002) 189–228.
[24] FactSage 6.3 – Summary of Databases. www.crct.polymtl.ca/fact/documentation./FSData.htm. (accessed March 2015).
[25] C.W. Bale, E. Bélisle, P. Chartrand, S.A. Decterov, G. Eriksson, K. Hack, et al., Calphad 33 (2009) 295–311.
[26] I. Alstrup, J.R. Rostrup-Nielsen, S. Røen, Appl. Catal. 1 (1981) 303–314.
[27] A. Lima da Silva, C.F. Malfatti, I.L. Müller, Int. J. Hydrogen Energy 34 (2009) 4321–4330.
[28] N.M. Hwang, J.H. Hahn, G.W. Bahng, Diam. Relat. Mater 3 (1993) 163–167.
[29] K. Hack, The SGTE Casebook: Thermodynamics at Work, CRC Press, Boca Raton, Fl, 2008.
[30] G. Eriksson, K. Hack, Metall. Trans. B 21B (1990) 1013–1023.

[31] Z. Cheng, H. Abernathy, M. Liu, J. Phys. Chem. C 111 (2007) 17997–18000.
[32] J.-H. Wang, M. Liu, Electrochem. Commun. 9 (2007) 2212–2217.
[33] J.W. Yun, S.P. Yoon, S. Park, H.S. Kim, S.W. Nam, Int. J. Hydrogen Energy 36 (2011) 787–796.
[34] J.W. Yun, S.P. Yoon, J. Han, S. Park, H.S. Kim, S.W. Nam, J. Electrochem. Soc. 12 (2010) B1825–B1830.
[35] C.J. Laycock, J.Z. Staniforth, R.M. Ormerod, Dalton Trans. 40 (2011) 5494–5504.